Journal of Rock Mechanics and Geotechnical Engineering 15 (2023) 2132–2146

Contents lists available at ScienceDirect

Journal of Rock Mechanics and Geotechnical Engineering

journal homepage: www.jrmge.cn

Full Length Article

Application of engineered compressible inclusions to mitigating soil-structure interaction issues in integral bridge abutments

Lila Dhar Sigdel [a,*], Minghao Lu [a], Ahmed Al-qarawi [b], Chin Jian Leo [a], Samanthika Liyanapathirana [a], Pan Hu [a]

[a] School of Engineering, Design and Built Environment, Western Sydney University, Kingswood, NSW, 2747, Australia
[b] Higher College of Technology, Abu Dhabi, United Arab Emirates

ARTICLE INFO

Article history:
Received 10 August 2022
Received in revised form
30 September 2022
Accepted 28 December 2022
Available online 15 March 2023

Keywords:
Integral bridge
Cyclic loading
Stress ratcheting
Settlement bump
Earth pressure distribution
Soil-structure interaction (SSI)

ABSTRACT

The thermally induced cyclic loading on integral bridge abutments causes soil deformation and lateral stress ratcheting behind the abutment wall due to the expansion and contraction of the bridge deck. The forward and backward movements of the abutment in response to the expansion/contraction of the bridge deck lead to the formation of settlement trough and surface heaving, frequently creating a bump at the bridge approach and increasing the lateral earth pressure behind the abutment. Measures to reduce the bump at the bridge approach, including several treatment methods, such as compaction of selected backfill materials, grout injection, installation of approach slab, and using a layer of compressible inclusion material behind the abutment were proposed. However, these guidelines still lack sufficient design details and there are limited experimental findings to validate design assumptions. In this paper, the use of engineered compressible materials to alleviate the lateral earth pressure ratcheting and settlement at the bridge approach is investigated. The comparative study is presented for the soil-inclusion, material-structure and soil-structure interactions for an integral bridge under three different backfill conditions, i.e. (a) sand, (b) sand and EPS geofoam, and (c) sand and Infinergy®. The study was conducted in a special large-scale test chamber with a semi-scale abutment to gain better insights into the soil-structure interaction (SSI). The kinematics and rearrangement of the soil during the cyclic loading have been investigated to identify the mitigating effects of compressible inclusions. The comparative study indicates that both compressible inclusions perform comparatively well, however, Infinergy® is a better alternative than the medium-density EPS geofoam, as it works more effectively to reduce the backfill settlement and heaving as well as soil ratcheting effects under cyclic translational movement.

1. Introduction

Integral bridges without expansion joints can reduce the construction and long-term maintenance costs typically associated with conventional bridge with expansion joints. Although the popularity of integral bridges has been increasing in many countries, there is still a discrepancy in design guidelines and design practices of integral bridges. The repetitive cyclic loading on integral bridge abutments is inherent due to the daily and seasonal temperature variations; consequently, the backfill soil wedge starts to slump downwards and towards the back of abutments, resulting in soil wedge failure during the contraction phase of the bridge deck. After the subsequent expansion of the bridge deck, the soil does not return to its original position, leading to a built-up of lateral earth pressure applied on the abutment (Springman et al., 1996; Ng et al., 1998; England et al., 2000; Goh, 2001; CosgroveLehane, 2003; Tapper and Lehane, 2005; Al-qarawi et al., 2020; Al-qarawi, 2021; Sigdel et al., 2021a). Therefore, especially during the annual summer expansion of the bridge deck, the developed lateral earth pressure due to the retained soil reaches a heightened state, resulting in a significantly higher lateral earth pressure compared to the earth pressure at the neutral position. The build-up of lateral earth pressure in this manner can cause structural distress. Another issue associated with cyclic thermal loading is the backfill surface settlement and heaving. With the increase in the number of cycles, settlement and heaving continue

* Corresponding author.
E-mail address: 18549889@student.westernsydney.edu.au (L.D. Sigdel).
Peer review under responsibility of Institute of Rock and Soil Mechanics, Chinese Academy of Sciences.

https://doi.org/10.1016/j.jrmge.2022.12.033

to develop, which will create a void at the face of the abutment resulting in an uneven bump at the bridge approach. If an approach slab is provided, the slab might crack due to the formation of the void underneath. Most current design guidelines have ignored the changes in backfill condition and provided little or no information particularly to rectify the settlement bump issue at integral bridges due to thermally induced cyclic abutment movement.

The primarily objective of this paper is to conduct a comparative study of the mitigation performance of two compressible inclusion materials in an integral abutment, one being a commonly used conventional compressible inclusion and the other a new potentially promising material. Therefore, the focus of this study is to investigate the use of the compressible materials to alleviate settlement issues and lateral earth pressure at the integral bridge abutment. The interactions at the integral bridge abutment incorporating two types of compressible inclusions, i.e. EPS geofoam and a new material, Infinergy® (a trademark of BASF), with the soil backfill were investigated. These results are also benchmarked against the case of not using any compressible inclusion to study the efficacy of each case.

2. Design of compressible inclusions

The studies on different polystyrene products, polyethylene foam, geocomposite materials, recycled tyre shreds, and rubbers have identified the potential of using these products as compressible inclusion behind an integral bridge abutment (Carder and Card, 1997, Horvath, 2000, Lee and Roh, 2007; Hazarika et al., 2008; Cui and Mitoulis, 2015; Argyroudis et al., 2016; DudaSiwowski, 2020). Integral bridge with reinforced backfill soil has also been investigated to mitigate the geotechnical issues in integral bridges (Tatsuoka et al., 2009; Munoz et al., 2012). A field study performed by Hoppe (2005) on a semi-integral bridge with the elasticised expanded polystyrene (EPS) at the integral backwall reported significant reductions in both the lateral earth pressure and observed settlement of the approach fill behind the abutments. However, Hoppe's study provided only limited backfill design configurations, and the design thickness of elasticised EPS geofoam is postulated based on the height of the backwall, and the total estimated lateral movement of the abutments. The findings are based on the monitored bridge over 5 years using the elasticised EPS of 250 mm thickness, which exhibits linear-elastic behaviour up to approximately 10% strain and linear (proportional) stress-strain behaviour up to about 30% strain with well compacted selected backfill material. It is advised that an elasticised EPS layer should be designed to perform within 10% strain during service (Hoppe, 2005). Virginia Bridge Design Manual (2020) included the design provisions for compressible inclusions behind integral bridge abutments based on Hoppe's study.

Colorado Bridge Design Manual (2023) states that a combination of mechanically reinforced earth (MSE) walls with a non-collapsible gap (between the MSE wall and the abutment) filled with low-density polystyrene is effective when reduced earth pressure effects are required. According to Utah Bridge Design Manual (2017), geofoam backfill is recommended as a measure to reduce or eliminate fill settlement behind the abutment. Pennsylvania Bridge Design Manual (2019) states that a 2 inches (50.8 mm) thick sheet of EPS geofoam is required against the entire area of the back face of the abutment to achieve a reduction in stress ratcheting. The passive earth pressure coefficient (K_p), equals to 4 should be used with the designed EPS layer, and $K_p = 12$ should be used for the structural backfill if there is no EPS layer. Virginia Bridge Design Manual (2020) states that a layer of EPS should be provided between the backfill and the abutment to minimise the effects of stress ratcheting due to thermal loading. The following guideline is given to calculate the thickness of the EPS layer, subject to a minimum thickness of 10 inches (25 cm):

$$EPS_t = 10(0.01H + 0.67\Delta L) \quad (1)$$

where H is the height of integral backwall/abutment in inches, ΔL is the total thermal movement in inches, and EPS_t is the EPS thickness in inches.

Only a few design guidelines have advised to use of compressible inclusions, particularly EPS geofoam, to reduce the effects of soil-structure interaction (SSI) issues in integral bridge abutments. However, available design guidelines are not consistent with each other and have provided little information about the geometric and material properties for the design of compressible inclusions. Although the aforementioned methods solve the problems to a certain extent, further investigations are necessary to develop effective solutions to resolve the approach settlement and stress ratcheting issues. The limited information available on the soil-material-structure, and SSI, make it difficult to utilise innovative backfill materials to design economical and durable integral bridge abutments.

3. Design of compressible inclusions

3.1. Physical modelling and similarity of model

The study in this paper investigated the interactions of an integral bridge abutment in a large-scale experimental facility. A semi-scale model of the integral abutment was designed based on dimensional analysis and by considering all relevant variables and developing dimensionless groups of those parameters to achieve stress and strain similarity with a prototype integral abutment twice its size (Al-qarawi, 2021). The following set of parameters governing the response of the integral abutment to temperature-induced displacement was assessed:

$$f = \{\sigma, \rho_1, g, H, c_1, \varnothing_1, \rho_2, c_2, \varnothing_2, E_1, E_2, \delta_w, S_i, n, E_p, d_p, l_p, I_p, \delta_p\} \quad (2)$$

where σ is the stress; ρ_1 and ρ_2 are the densities of soil-1 (soil adjacent to the abutment) and soil-2 (soil adjacent to the pile if any), respectively; H is the retained height of the soil (in this case equal to the wall height); g is the gravitational acceleration; c_1, $\varnothing_1$, c_2 and $\varnothing_2$ are the shear strength parameters of soil-1 and soil-2, respectively; E_1 and E_2 are the elastic moduli of soil-1 and soil-2, respectively; δ_w and δ_p are the friction angles at the soil-wall and soil-pile interfaces, respectively; S_i is the wall displacement; n is the number of movement cycles; and E_p, d_p, l_p and I_p are the elastic modulus, diameter, length and moment of inertia of the cross-section of the pile (if used), respectively.

According to the dimensional analysis, density of the soil in the experimental model with a scale of 1:2 to the prototype ($H^m = H/2$, where H^m is height of the model abutment wall) and normal gravity ($g^m = g$) must be equal to two times that in the prototype to replicate the similar stress levels as in the full-scale prototype. In this study, the experiments were conducted under normal gravity condition ($g^m = g$), where the height of the model abutment wall (H^m) was 0.96 m, half that of prototype wall height ($H = 1.92$ m). Material selection for the semi-scale model to achieve similarity with the prototype is discussed below.

3.2. Materials

3.2.1. Soil

To replicate the similar stress levels as in the full-scale prototype, the density of the material replicating soil should be equivalent to twice that of the soil in the prototype. Black sand, also named Iron sand, was considered as a suitable model backfill material for the experiment. It is a natural granular material formed by the deposition of volcanic debris from offshore volcanos. The proposed Black sand (dry density ~3000 kg/m^3), is twice as heavy as the typical approach backfill soil (dry density 1400–1500 kg/m^3) and possesses similar shear strength parameters, cohesion (c) and angle of internal friction (φ) and Young's modulus (E_s) compared to typical backfill soils.

The maximum density test (ASTM D4253-16e1, 2016) and minimum density test (ASTM D4254-00, 2000) were conducted for the Black sand. Its maximum and minimum densities were determined as $\rho_{max} = 3278$ kg/m^3 and $\rho_{min} = 2690$ kg/m^3 respectively. Sieve analysis (Fig. 1) showed that the particle size of Black sand ranging from 75 μm to 0.3 mm. The diameter corresponding to 50% finer in the grain size distribution, D_{50}, is 0.132 mm. Based on the shear box and triaxial tests conducted at different relative densities, it is found that the residual and peak friction angles vary from 32° to 43° for the relative density in the range of 4.5%–73.5%, respectively.

3.2.2. Compressible wall inclusion

EPS geofoam is the most common compressible inclusion recommended by many design practices and has been studied by many researchers (Horvath, 1997; Leo et al., 2007; Al-qarawi et al., 2016; Gade and Dasaka, 2022). However, in this paper, a new material called "Infinergy®" (manufactured by BASF) is studied with EPS geofoam in a comparative assessment of performance. Both are also benchmarked against the "no inclusion" case. There is little or no information in the literature about applying Infinergy® as a construction material. Before the experiments, uniaxial compression and hydrostatic compression tests were carried out for both Infinergy® and EPS geofoam to investigate the constitutive behaviour. Figs. 2 and 3 illustrate the material behaviour under loading for EPS geofoam and Infinergy®, respectively. Mechanical properties derived from the experiments are summarised in Table 1.

Based on the experiments, it is found that the compressive strength at 10% strain is 96 kPa for the EPS geofoam and 50 kPa for the Infinergy®. The elastic modulus of the Infinergy® is approximately 10 times less than that of the EPS geofoam. EPS geofoam behaves as a linear elastic material up to a strain of about 1.8%,

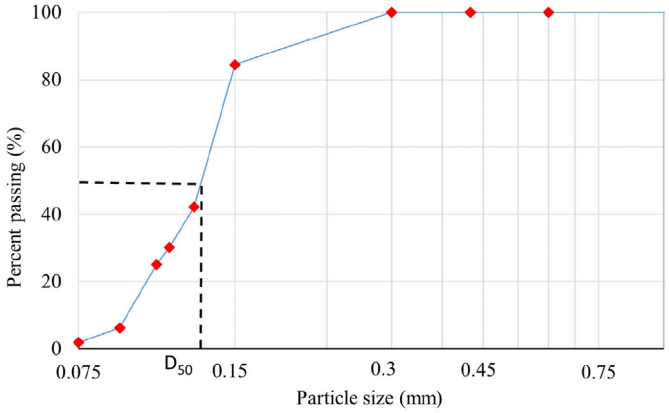

Fig. 1. Particle size distribution for Black sand.

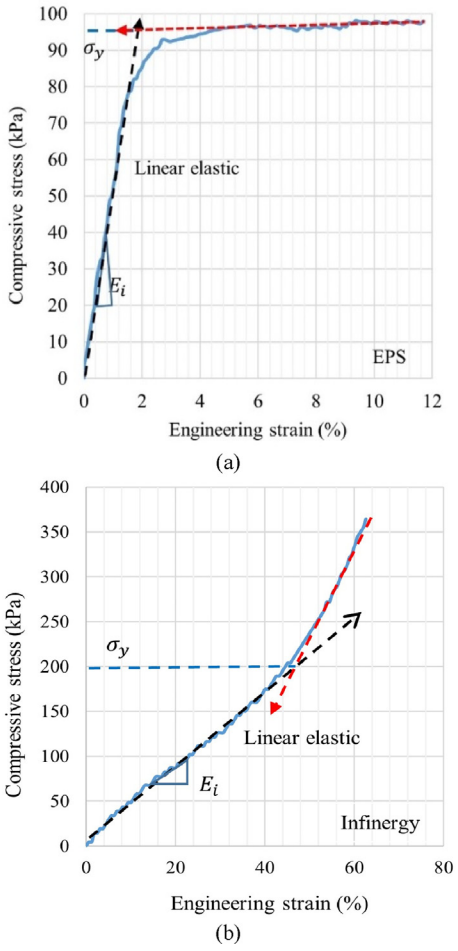

Fig. 2. Unconfined compression test for (a) EPS geofoam and (b) Infinergy®.

whereas Infinergy® behaves as a linear elastic material up to a strain of about 45%, which is about 25 times higher than EPS geofoam. Unit weight of EPS geofoam is 11.5 times less than that of Infinergy®. Therefore, it can be concluded that Infinergy® is highly elastic in behaviour and less stiff than EPS geofoam. In addition, Infinergy® is 11.5 times heavier than the EPS geofoam, and about 6.5 times lighter than typical soil used as a backfill material (1400–1500 kg/m^3).

Although the Infinergy® is a new material, studies by Ge et al. (2017) and Jiang et al. (2022) have shown it has high fatigue threshold, high abrasion and good chemical resistance. A 200 cyclic compression test at 60% strain (beyond its elastic limit of 45%) conducted by Ge et al. (2017) showed that the Infinergy® samples recover on the average more than 95% both in stress and compression modulus, after samples have been allowed to recover for 24 h, 3 d and 6 d. Scanning electron microscopy (SEM) tests carried out on the samples before and after the test have shown no significant damage to either the cell structure or the inter-bead bonding, and a low shrinkage ratio of only about 0.7%. Infinergy® has a rebound (energy return) of about 55%, whereas for commercially available EPS Geofoam it is less than 20% (Prissok et al., 2010). A variety of Infinergy® applications from footwear to athletics track, playground and motorcyclist helmet can be found. A tensile strength test conducted by Ge et al. (2017) on Infinergy® indicated a high tensile strength of 1.8 MPa and an elongation at a break of 360.1%, which is much higher than that for commercially available EPS geofoam (<15%).

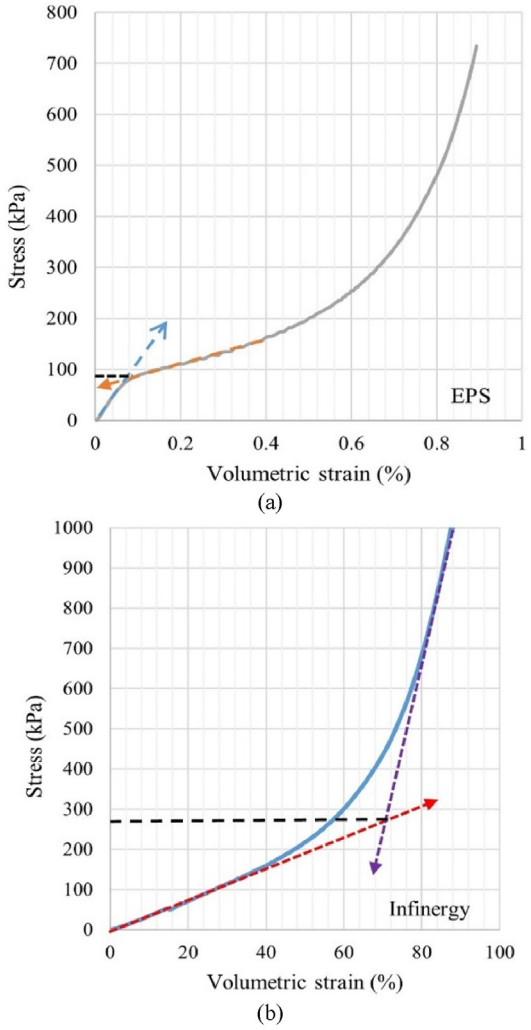

Fig. 3. Hydrostatic compression test for (a) EPS geofoam and (b) Infinergy®.

SEM tests were carried out to study the microstructure of the EPS geofoam and Infinergy® samples. The internal structure of the EPS geofoam (density = 20 kg/m^3) and Infinergy® (density = 230 kg/m^3), magnified by 160 times and the electron beam operated using a 25 kV charge, is shown in Fig. 4. The internal structure of EPS geofoam is composed of fused thinner translucent closed cell walls. Also, the SEM micrographs of the EPS sample show a dense honeycomb structure with irregular internal voids and cell wall thickness. Infinergy® has a less dense honeycomb structure with thicker cell walls and larger internal voids.

3.3. Experimental set-up

3.3.1. Model facility

The model tank of the experimental facility with a moveable abutment wall controlled by actuators on the left is shown in Fig. 5. It has dimensions of 3 m × 1.5 m × 1.2 m (length × breadth × height). The size of the tank was determined based on the three-dimensional (3D) finite element modelling (FEM) conducted by Al-qarawi (2021). It was designed in such a way that any potential failure surface during experiments would not be intersected and affected by the tank boundaries. Also, the tank width is chosen to be sufficient so that the total frictional force from the sides of the tank is insignificant compared to the lateral soil thrust.

The wall has an actual height of 1.1 m, which could simulate up to a 2.2 m high abutment on a field scale. However, in these experiments, the height of the backfill retained by the abutment was set up to 0.96 m, which is equal to a 1.92 m high abutment on a field scale. The front side of the tank consists of a 25-mm thick transparent perspex and the back side of the tank is made of a 5-mm thick steel sheet. Both walls are braced by vertical and horizontal steel frames. A perspex sheet of 5 mm in thickness is also attached to the back side steel wall to reduce the wall friction and to simulate the same conditions as at the front side perspex wall. The rear end wall of the tank is made of a 25-mm thick steel sheet braced by vertical and horizontal steel frames. The abutment wall is 50-mm thick braced with vertical, horizontal, and diagonal steel frames at the actuator side, and attached with 40-mm thick transparent perspex at the soil side. Pressure transducers were mounted on the 40-mm thick perspex sheet. The abutment wall sits on a metal sheet at 50 mm above the floor of the tank.

3.3.2. Instrumentation

Four electronic actuators were attached to the abutment wall and fixed to the vertical frame at the other end (see Fig. 5). A software module controls the four actuators and can be programmed to effect translational, rotational, or mixed translational and rotational movements in both active and passive directions. Each actuator has a maximum load capacity of 150 kN, load accuracy of ±1%, inbuilt linear variable differential transformer (LVDT), and one external LVDT attached outside the actuator. The minimum speed limit of the actuators is 0.005 mm/min, and the maximum speed limit is 50 mm/min, with an actuator stroke length of 200 mm (±100 mm). The system can also be controlled by either displacement or load.

Five pressure transducers were installed at the abutment wall, facing the backfill to record the lateral earth pressure distribution during the experiment. The bottom pressure transducer was installed at 10 mm from the bottom of the wall, and the rest of the pressure transducers are equally spaced at 200 mm. Also, one pressure transducer is installed at the rear end wall, which is at the opposite end to the abutment, to make sure that the measured readings at the abutment end are free of boundary effects. The readings from the pressure transducers are recorded in a computer using a data logger.

3.3.3. Sand filling

The model tank was filled with Black sand using two powerful motors and dispersed directly from the top of the tank, which is 1.2 m height from the bottom of the tank. Because of the high blown power, falling height is kept constant throughout the sand loading process. The filling method is kept consistent for all experiments with and without an Infinergy® compressible inclusion. Although the motors were fixed in their position, due to the high wind speed generated by the motors, sand was dispersed all around

Table 1
Material properties for EPS geofoam and Infinergy®.

Material type	Density (kg/m^3)	Elastic modulus (kPa)	Yield stress (kPa)	Compressive strength at 10% strain (kPa)
EPS geofoam	20	4550	95	96
Infinergy®	230	435	210	50

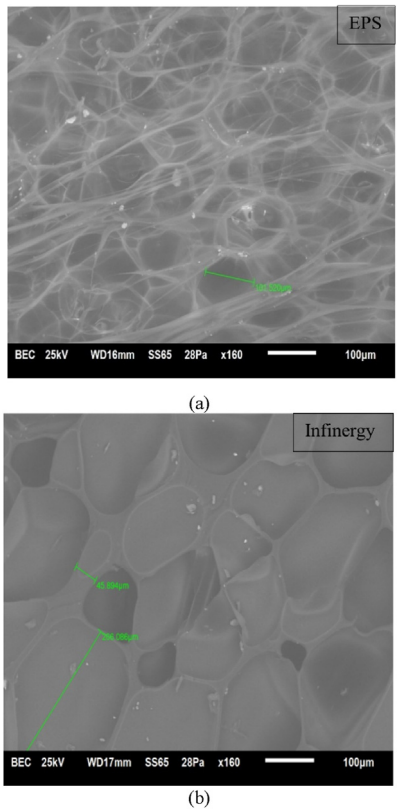

Fig. 4. SEM images for (a) EPS geofoam and (b) Infinergy®.

the tank during filling, and a relatively denser backfill is created. The experiment with EPS geofoam as a compressible inclusion was conducted by Al-qarawi (2021), and a manually operated mobile sand raining system was used to deposit the sand inside the tank, which is different from the motor-driven system described above. Hence, relative densities of the backfill inside the tank were determined as 79.8%, 78.4%, and 25.6%, respectively for experiments with three different backfill conditions: (a) Experiment 1, sand only; (b) Experiment 2, sand and Infinergy®; and (c) Experiment 3, sand and EPS geofoam.

3.3.4. Experimental cases

Experiments 1 and 2 were identical in terms of the speed of the wall movement, backfill density, and the total number of cycles of the experiment, as shown in Table 2. Experiment 3 by Al-qarawi (2021) was conducted only up to 50 cycles. For the initially designed large-scale testing chamber, 50 cycles was the limit the experiments could have been conducted due to mechanical constraints, therefore, comparative experiments between Infinergy® and EPS geofoam was planned for 50 cycles before our large-scale testing chamber was updated. The EPS geofoam testing was conducted using the old version of the test chamber. Following updating of the test chamber after the EPS geofoam experiment, testing could be extended to 120 cycles with installation of powerful actuators. Since Infinergy® is a new material used for this kind of application and found to produce good results at 50 cycles, it was then decided to subject the performance of Infinergy® to more rigorous loading by extending the test to 120 cycles. For sake of comparison, Experiment 1 (no inclusion, sand only) was also extended to 120 cycles. The wall movement for Experiment 3 was

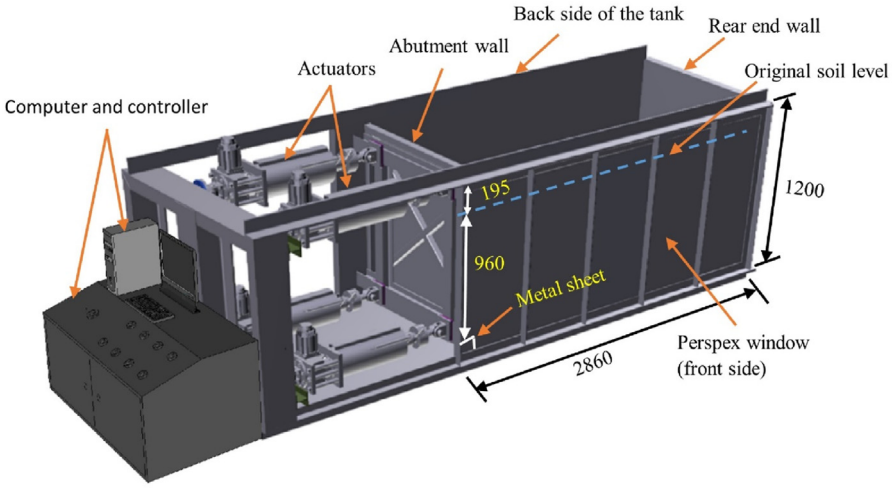

Fig. 5. Model tank with the semi-scale abutment wall located on the left (Note: all dimensions are in mm).

Table 2
Test conditions of the experimental cases.

Test No.	Backfill	Speed (mm/min)	Displacement/height, $\pm\Delta/H$ (%)	Total time (h)	Relative density, D_r (%)	Number of cycles	Source
Experiment 1	Sand only	2.5	1	32	79.8	120	This study
Experiment 2	Sand plus Infinergy®	2.5	1	32	78.4	120	This study
Experiment 3	Sand plus EPS geofoam	2.6	1	12.5	25.6	50	Al-qarawi (2021)

Note: The abutment displacement in Experiments 1–3 is ±10 mm.

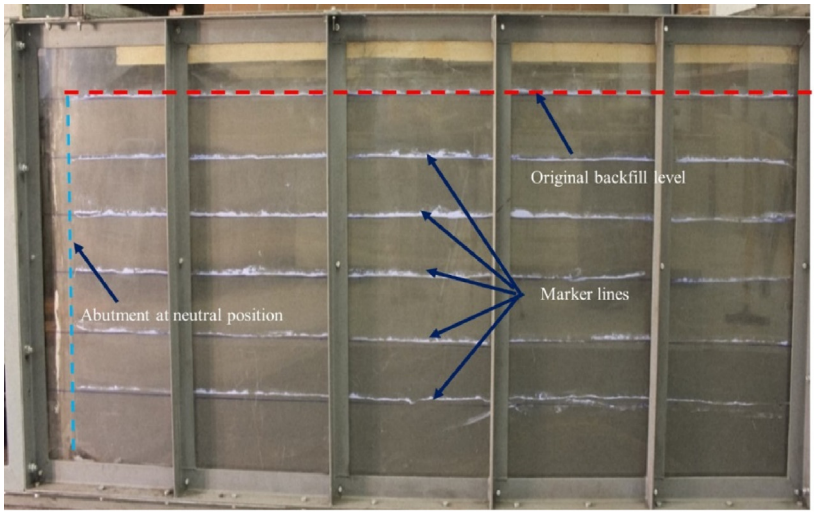

(a)

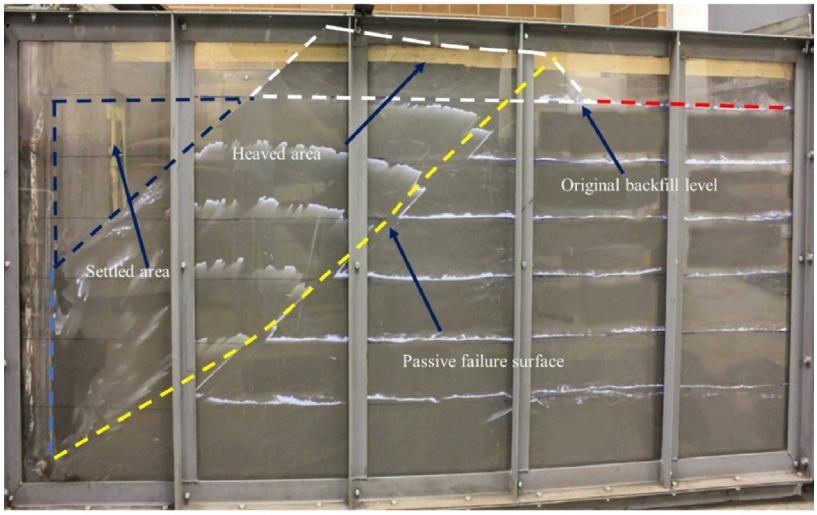

(b)

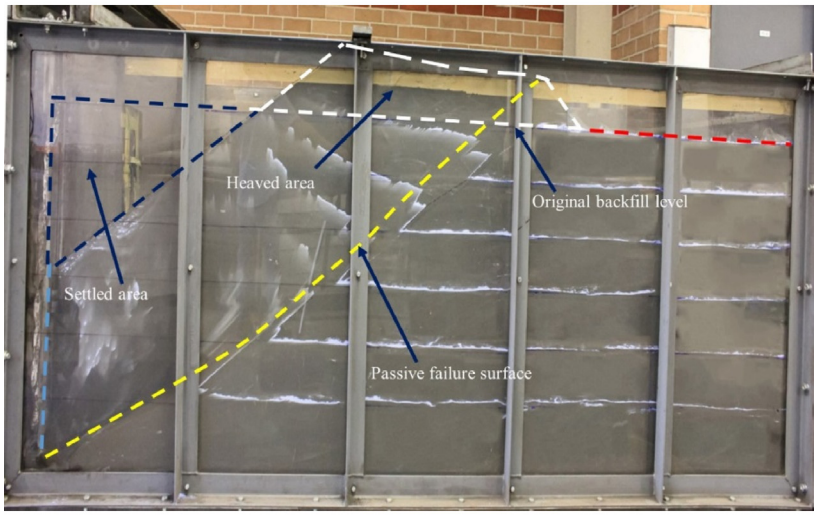

(c)

Fig. 6. Backfill profiles at neutral position: (a) At zero cycle, (b) After 50 cycles, and (c) After 120 cycles.

performed manually. Hence, the rate of wall movement was slightly different compared to the first two experiments. Since the design life of an integral bridge varies from 75 years to 120 years (e.g. 75 years in the USA, 120 years in the UK and 100 years in Australia), these experiments were conducted for 120 cycles corresponding to 120 cycles of seasonal changes.

4. Results and discussion

4.1. Results from the three experiments

4.1.1. Experiment 1

In this test, the wall was moved in a cyclic translational movement, and 120 cycles of 10 mm displacement amplitude at a rate of 2.5 mm/min were applied. This would correspond to a ±20 mm cyclic displacement in the prototype. PD 6694-1 (2020) has advised that for 40 mm of (total) integral bridge deck movement, if the bridge is symmetrical in shape, and the foundation condition is identical for each abutment, the design displacement for each integral abutment will be 20 mm, and in that condition, an integral abutment can be designed using the limit equilibrium approach. The allowable maximum bridge length for the design of integral bridge is 60 m in some countries, i.e. UK, New Zealand and Australia (Sigdel et al., 2021b). In accordance with the AS 5100:2017 (2017), by considering the maximum air temperature of 55 °C and 45 °C for the superstructure of steel deck on steel beams, and concrete deck on steel beams, respectively, the anticipated thermal displacement at the end of the bridge deck for an integral bridge of 60-m span length would be 19.3 mm for steel bridge and 14.6 mm for the concrete bridge. Hence the choice of ±10 mm abutment displacement in these experiments (or ±20 mm in field scale) covers the upper bound abutment displacement of a majority of integral bridges of 60 m span or less. Soil deformation behind the abutment was recorded at three different positions of the wall during every cyclic movement (active, passive, and neutral). The earth pressure distribution was recorded at an interval of 10 s. Images were taken at each loading cycle of the experiment, and marker lines were placed to observe the failure surface during the experiments. The initial and final backfill conditions after 50 cycles and 120 cycles are shown in Fig. 6. Backfill profiles behind the wall after 25 cycles, 50 cycles, and 120 cycles of translational movement are shown in Fig. 7.

The soil behind the abutment slumped down from the original ground surface in front of the wall, and soil heaving was observed. The soil profiles in Fig. 7 show that the maximum soil settlement near the abutment remained the same after 50 cycles. However, the heaving along the surface had changed slightly between 50 and 120 cycles. The maximum vertical soil settlement adjacent to the abutment after 25 cycles was 325 mm. After 50 cycles, it was 410 mm, showing that the maximum total settlement increased by only 21% after 25 cycles. These results show that the degree of settlement increases with an increasing number of cycles up to a certain number of cycles and after that, it reaches a residual settlement value.

The amount of soil heaving also increases with the number of loading cycles. After 25 cycles, the maximum height of the heave reached 85 mm, which was measured above the original soil surface. It was 180 mm after 50 cycles and 195 mm after 120 cycles. It shows that the rate of soil heaving increases with the number of cycles only up to a certain number of cycles and then starts to decrease. The measured area of the settlement trough behind the abutment was 0.14 m^2 and the heaved area was 0.16 m^2 after 120 cycles. The total volume of heaving soil deposited away from the abutment was slightly higher than the total volume of soil settlement trough behind the abutment. The passive earth pressure distributions along the height of the abutment at the 25th cycle, 50th cycle, and 120th cycle are presented in Fig. 8, and the

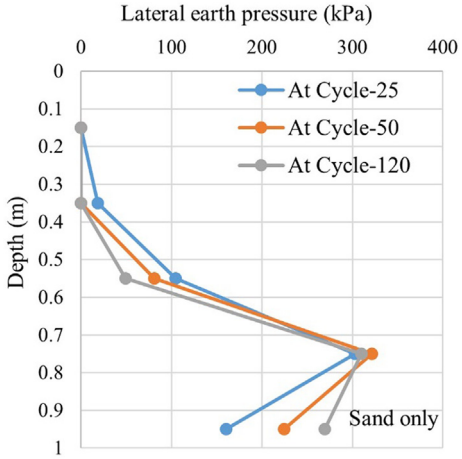

Fig. 8. Distributions of passive pressure along the height of the wall at the 25th cycle (Cycle-25), 50th cycle (Cycle-50), and 120th cycle (Cycle-120).

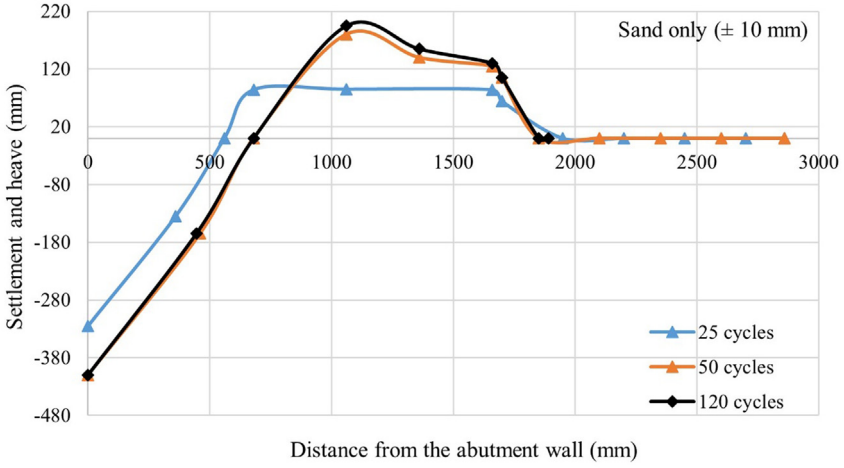

Fig. 7. Backfill profiles along the surface at different cycles.

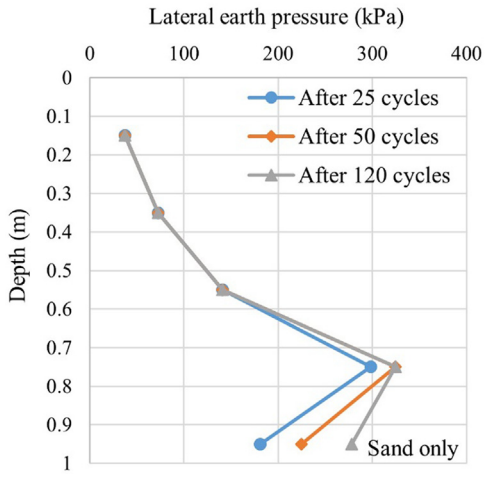

Fig. 9. Distributions of maximum earth pressure envelope along the height of the wall until 25 cycles, 50 cycles, and 120 cycles.

maximum earth pressure envelopes after 25 cycles, 50 cycles, and 120 cycles are presented in Fig. 9.

Fig. 8 captures the maximum pressure distributions at the 25th (Cycle-25), 50th (Cycle-50) and 120th cycles (Cycle-120). It is observed that at the top part of the abutment, the pressures recorded by the top three pressure cells were higher at Cycle-25 than those at Cycle-50 and Cycle-120. In fact, the top two pressure cells recorded zero reading at Cycle-50 and Cycle-120. This is because the depth of the settlement trough after 50 cycles had fallen below the level of these two pressure cells. The maximum pressure envelope in the top part of the abutment was therefore established before Cycle-50. However, in the lower part of the abutment, the pressures at Cycle-50 and Cycle-120 exceeded those of Cycle-25 indicating that following the soil circulation, the passive load was redistributed to the lower part of the abutment at Cycle-50 and Cycle-120. The maximum pressure envelope in the lower part of the abutment was therefore established after Cycle-50.

Fig. 9 shows the full maximum earth pressure envelope after Cycle-25, Cycle-50 and Cycle-120. It shows that the effect of several cycles on the maximum lateral earth pressure envelope over the upper part of the abutment (to a depth of 0.55 m below the initial soil surface) was insignificant. Lateral earth pressure increased slowly after 25 cycles in the bottom lower region of the abutment (0.55–0.96 m below the initial soil surface). The maximum passive pressure at the bottom transducer (0.95 m) increased with the number of loading cycles. This may be due to the soil densification progressing towards the bottom of the wall because of soil slumping. The maximum passive earth pressure of 324.3 kPa was observed at 0.75 m below the original ground level of the backfill during the experiment. According to these results, the maximum earth pressure distribution over the bottom lower part of the abutment will increase continuously during the cyclic translational movement. These results confirm that the earth pressure distribution is not a triangular shape as suggested by PD 6694-1 (2020) for integral bridge abutments under cyclic translational wall movements.

4.1.2. Experiment 2

Thirty sheets of Infinergy® with dimensions of 0.12 m × 0.5 m × 0.03 m (length × breadth × height) were glued together to form a block with a thickness of 0.3 m and fitted inside the model tank over the inner surface of the abutment as shown in Fig. 10. Sand filling in the tank was carried out in the same manner as in the Experiment 1. The test configuration and data recording were similar to Experiment 1 (Table 2). The final backfill conditions after 50 cycles and 120 cycles of ±10 mm cyclic translational movement are shown in Fig. 10. Backfill profiles behind the wall after 25 cycles, 50 cycles, and 120 cycles of translational movement are plotted in Fig. 11.

There was no deposition (i.e. heaving) of the sand above the original backfill level, and the maximum settlement and settlement trough area was considerably less than in the Experiment 1. Because the thickness of the compressible inclusion was 300 mm, the horizontal axis in Fig. 11 started from 300 mm. Fig. 11 shows that 79% of the maximum settlement (60 mm) occurred before the 25th cycle, and the effects of loading cycles were insignificant after 25 cycles. Also, 85% of the total settlement (65 mm) occurred before the 50th cycle. It shows that the rate of soil settlement increased with the number of cycles only up to a certain number of cycles and started to decrease after that.

The increase in lateral earth pressure with an increase in the number of cyclic loading was insignificant, and maximum passive pressure was increased by only 5 kPa from 25 cycles to 120 cycles (see Fig. 12). Because there was no significant difference in passive earth pressure at different cycles, only the maximum earth pressure envelope is presented here. The maximum earth pressure observed in Experiment 2 was 46 kPa at 0.75 m below the initial soil surface which was approximately seven times less than the maximum earth pressure recorded in Experiment 1. The maximum earth pressure recorded for Experiment 2 was only 22% of the yield stress of the Infinergy®.

4.1.3. Experiment 3

In this test, the wall was moved in the translational movement for a total of 50 cycles of ±10 mm displacement amplitude at a rate of 2.6 mm/min (Al-qarawi, 2021). Block of medium-stiffness EPS geofoam of 600 mm in thickness was used as a compressible inclusion between the soil and wall. This experiment was conducted in a different experimental set-up (see Table 2), and the results cannot be compared directly with Experiments 1 and 2. Therefore, results have been adjusted to match the experimental conditions of Experiments 1 and 2, and discussed in the following section. The backfill conditions, backfill profiles, and maximum earth pressure envelopes at 25 and 50 cycles are presented in Figs. 13–15, respectively.

Because the total thickness of the EPS block was 600 mm, the horizontal axis in Fig. 14 starts from 600 mm. Results show that the maximum settlement closer to the abutment increased by only about 23% between the 25 cycles (135 mm) and 50 cycles (175 mm). Similar to Experiments 1 and 2, the rate of soil settlement increased with the number of cycles only up to a certain number of cycles and started to decrease after that. This indicates that the settlement is likely to reach a residual state eventually on this projected trend. As in Experiment 2, heave was not developed behind the abutment wall.

Only three pressure transducers were installed in Experiment 3, therefore, pressures were recorded only at three locations along the height of the abutment. Because there was only a marginal difference in passive earth pressure for a different number of cyclic loading, only the maximum earth pressure envelopes are presented here. Fig. 15 shows that the lateral earth pressure becomes independent of the number of cycles and reaches a residual value without any signs of ratcheting between 80 and 90 kPa. The maximum earth pressure observed in Experiment 3 was 90 kPa which was approximately 28% of the maximum earth pressure recorded in Experiment 1.

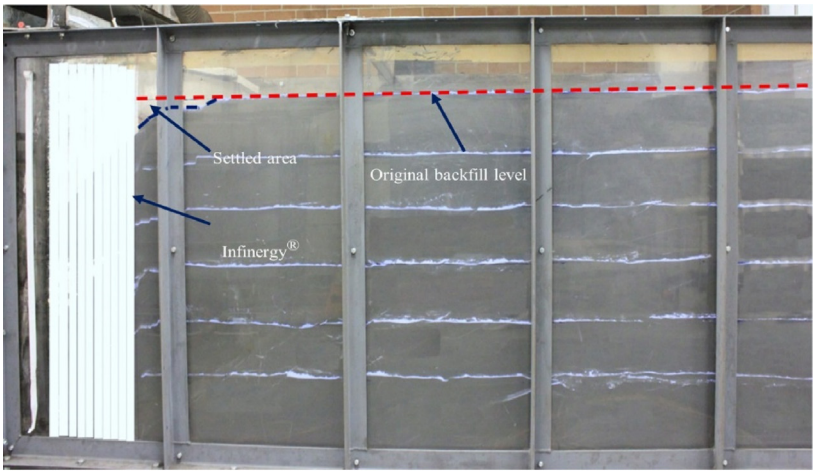

(a)

(b)

Fig. 10. Backfill profiles at neutral position after (a) 50 cycles and (b) 120 cycles.

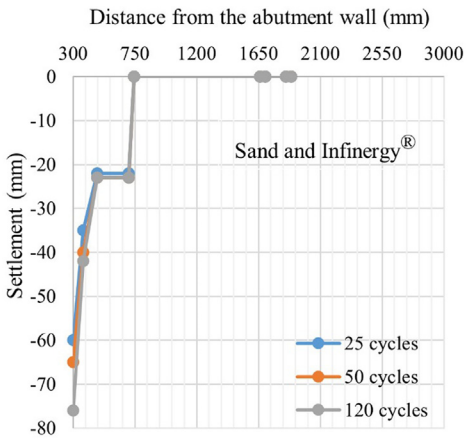

Fig. 11. Backfill profiles at different cycles.

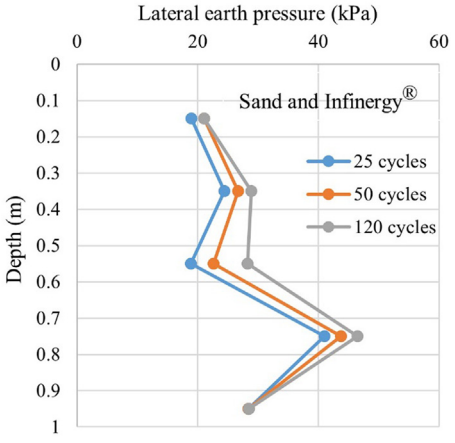

Fig. 12. Distributions of maximum earth pressure envelope along the height of the wall until 25 cycles, 50 cycles, and 120 cycles.

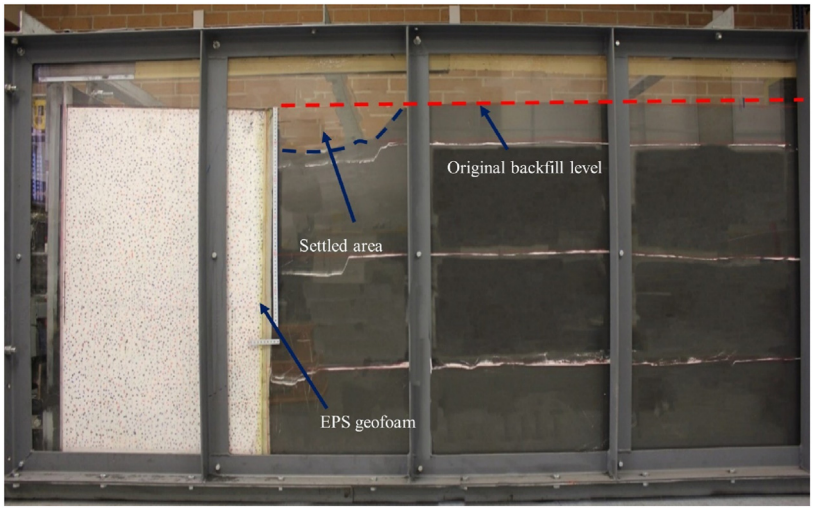

Fig. 13. Backfill condition after 50 cycles (at neutral position) (Al-qarawi, 2021).

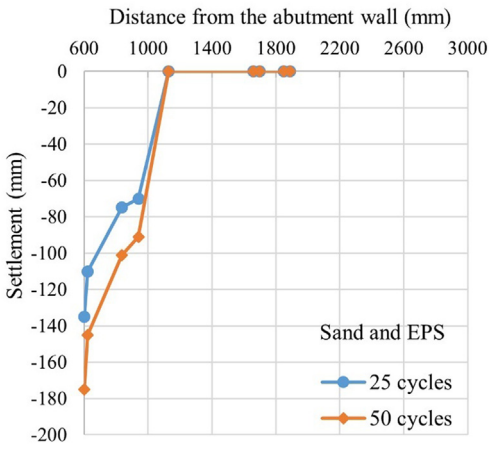

Fig. 14. Backfill profile at different cycles.

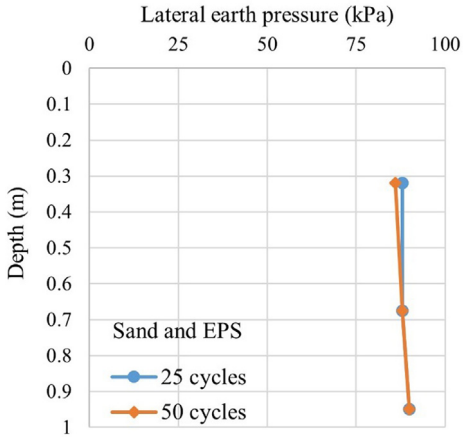

Fig. 15. Distributions of maximum earth pressure envelope along the height of the wall until 25 cycles and 50 cycles.

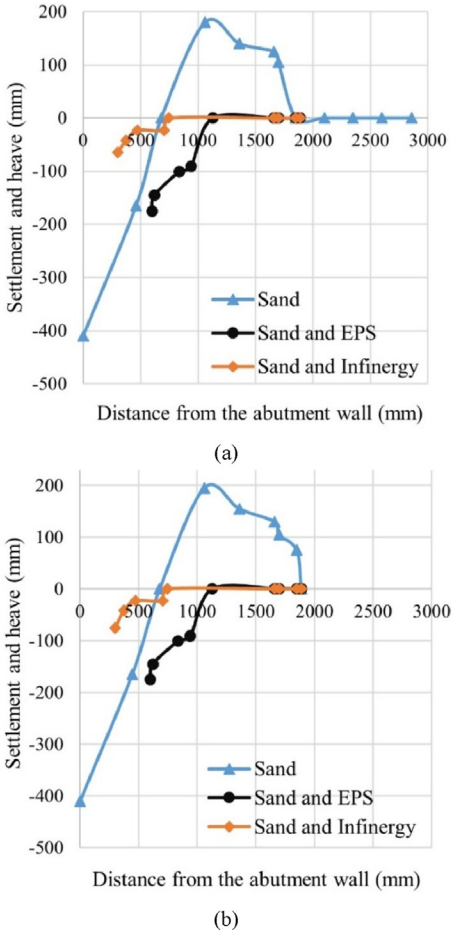

Fig. 16. Backfill profiles: (a) After 50 cycles, and (b) At the end of experiments.

4.2. Comparison of results from the three semi-scale experiments

4.2.1. Soil deformation

The backfill profiles after 50 cycles of each experiment and at the end of the experiment (after 120 cycles for Experiments 1 and 2, and after 50 cycles for Experiment 3) are shown in Fig. 16. The

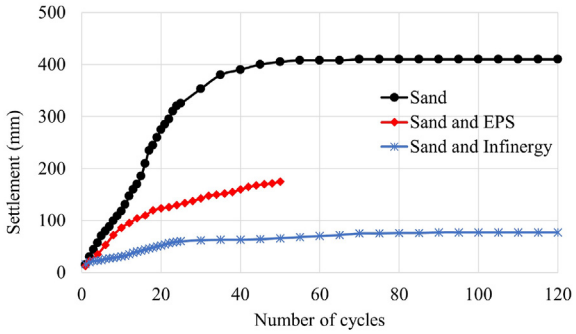

Fig. 17. Maximum settlement near the edge of the abutment (at the interface of abutment and soil, or the interface of inclusion and soil) with a number of cycles.

maximum settlement near the abutment with respect to the number of loading cycles is shown in Fig. 17. It is found that the Infinergy® perform better than the EPS geofoam, as observed from the results presented in Figs. 16 and 17. Because the relative density of the soil in the same semi-scale model tank was different for Experiment 3, the settlement values from Al-qarawi (2021) have been adjusted to normalise the findings from the three experiments to the identical situation for all three experiments, as shown in Table 3.

Since the maximum developed earth pressure behind the abutment in Experiment 3 was approximately equal to the yield stress of the EPS geofoam, and the value started to stabilise even before the 50th cycle, only adjustment for the soil settlement in Experiment 3 is deemed necessary. The (downwards) adjustment factor of 0.88 was estimated by benchmarking the settlement results over 20 cycles from Al-qarawi (2021) for ±10 mm cyclic translational movement for sand only case (no compressible inclusion) against those of Experiment 1.

A comparison between Al-qarawi's and Experiment 1's settlement results shows a strong correlation between compaction level and settlement behind the abutment. Both have a similar experimental set-up except for the relative density of the backfill. These findings are also reported by other investigators (Hoppe, 2005; Aziman et al., 2019; Gade and Dasaka, 2022). Applying the adjustment factor to accounting for different relative densities, the total settlement for Experiment 3 was therefore reduced to 154 mm (compared to the original settlement of 175 mm) at the end of 50 cycles. With the revised value, Infinergy® still performed better in respect of the maximum soil settlement in being less than 50% of that of the EPS geofoam for the first 20 cycles (52 mm versus 109 mm), and even better with an increase in the number of cycles. It also shows that Infinergy® reduced the maximum settlement to only about 16% of that without any inclusion, whereas EPS geofoam reduced it to about 38% of the same "no inclusion" benchmark, in all cases for the first 50 cycles.

The total area of settlement trough after 50 cycles and 120 cycles with Infinergy® reduced to about 8.4% and 8.6% of that without any inclusion, respectively at the same number of cycles. After 50 cycles, the settlement trough area with EPS geofoam (0.065 m^2) was approximately 46% of that for the no inclusion case (0.14 m^2). Therefore, in terms of the maximum settlement and settlement trough area behind the abutment, Infinergy® performed better even with the thickness being equal to half of the thickness of EPS geofoam used in Experiment 3.

Soil movement behind the abutment during the cyclic translational movement of 120 cycles without an inclusion layer and with an inclusion layer is presented in Fig. 18. The vector plot of the soil deformation was obtained using the open-source software modules (OpenPIV) for Particle Image Velocimetry (PIV) image analysis and post-processing of images captured during the experiments (Liberzon et al., 2021).

Active slip surfaces in Experiment 1, which changed with cycles of loading, and a passive failure surface which started to appear at later cycles were both clearly observed (Fig. 18). After a certain number of cycles, the settlement in Experiment 1 stabilised. The soil particles near to the abutment started to circulate around. Nevertheless sand particles were also moving in an upward direction. However, only the active slip surfaces due to slumping of soil particles with an increase in number of cyclic loading were observed in Experiment 2 (sand and Infinergy®). There was no clear passive failure surface developed during Experiment 2. This could be because the soil settlement stabilises due to the mitigation effects of the compressible inclusion on the SSI after a certain number of cycles.

4.2.2. Lateral earth pressure distribution

The variation of maximum earth pressure coefficient along the height of the abutment for all three experiments up to 50 cycles, together with the at-rest lateral earth pressure coefficient (K_0) from Experiment 1 are shown in Fig. 19. The lateral earth pressure coefficient ($k = \sigma_{hmax}/\sigma_{vo}$) along the height of the abutment is plotted with respect to the normalised depth (Z/H). Here, σ_{hmax} is the maximum lateral earth pressure, σ_{vo} is the initial vertical stress, Z refers to the depth of the soil from the surface, and H refers to the total backfill height. Furthermore, passive earth pressure coefficient (K_p) was calculated for residual and peak friction angles (32° and 43°) based on the shear box and triaxial test results of the Black sand at different relative densities and presented together in Fig. 19. The passive earth pressure coefficient was calculated using the log-spiral solution developed by Al-qarawi et al. (2021), which applies to the retaining wall structure under monotonic loading.

The graph shows that the maximum lateral earth pressure coefficient recorded without any compressible inclusion is 13.6, which is 3 times and 1.6 times higher than the maximum lateral earth pressure coefficient recorded in Experiment 2 (sand and Infinergy®) and Experiment 3 (sand and EPS geofoam), respectively. Moreover, the conventional passive pressure coefficient, K_p, based on monotonic loading does not accurately predict the passive lateral pressure caused by cyclic abutment wall movements.

The maximum earth pressure envelopes obtained from these three experiments have been compared with design guidelines used in practice: PD 6694-1 (2020), Utah Bridge Design Manual (2017), MassDOT (2020), CAN/CSA-S6-14 (2015), Pennsylvania Bridge Design Manual (2019), and presented in Fig. 20. For PD 6694-1 (2020), earth pressure distribution was calculated for two values of peak friction angles (32° and 43°). Most of the current design practices seem to underestimate the maximum lateral earth pressure. Only the earth pressure distribution calculated using PD 6694–1 for a friction angle of 43° was close at the lower bottom part of the abutment (at 0.78 m below the original soil level), whereas for the upper part PD 6694–1 overestimates the lateral earth pressure. These results emphasised the fact that the use of a right triangular passive pressure distribution based on any of the current design practices does not replicate the lateral earth pressure distribution in integral bridge abutments under cyclic translational movements.

4.2.3. Effects of Infinergy® layer in mitigating the displacement of abutment

Experimental evidence suggests that the 300 mm thick Infinergy® performed better than the 600 mm thick EPS geofoam of medium density, with respect to the significant reduction of the soil settlement and lateral earth pressure behind the abutment. To

Table 3
Comparison of settlement data.

Experiment type	Relative density, D_r (%)	Total cycles	Maximum settlement (mm)	Settlement at the 20th cycle	Adjusted settlement at the 20th cycle ($D_r \approx 80\%$)	Adjusted settlement at the 50th cycle ($D_r \approx 80\%$)	Area of settlement trough at the 50th cycle (m^2)
Sand only (Al-qarawi 2021)	25.6	20	313	313	275	N/A	N/A
Experiment 1	79.8	120	410	275	275	410	0.14
Experiment 2	79.5	120	76	52	52	76	0.012
Experiment 3	25.6	50	175	124	109	154	0.065

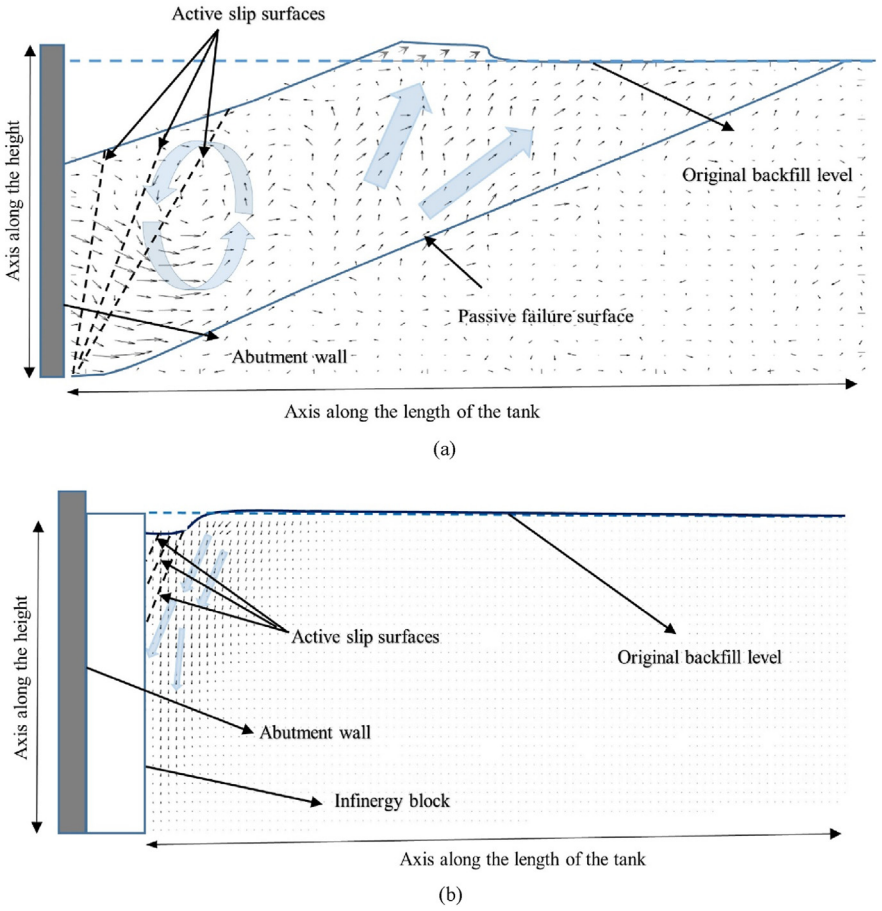

Fig. 18. Vector plots of sand movement in (a) Experiment 1 (sand only), and (b) Experiment 2 (Infinergy® and sand).

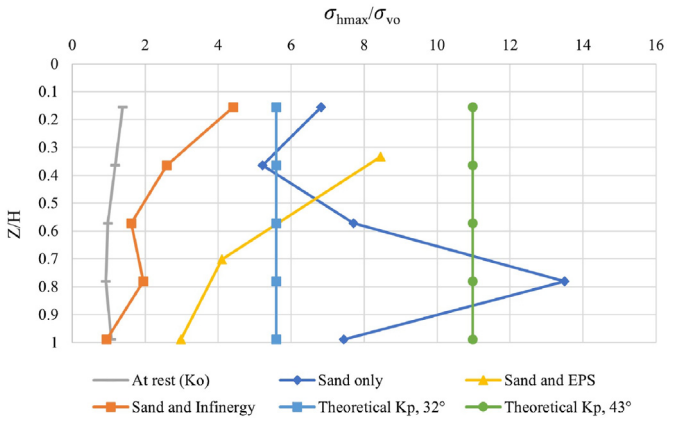

Fig. 19. Variations of maximum lateral earth pressure coefficient along the height of the wall.

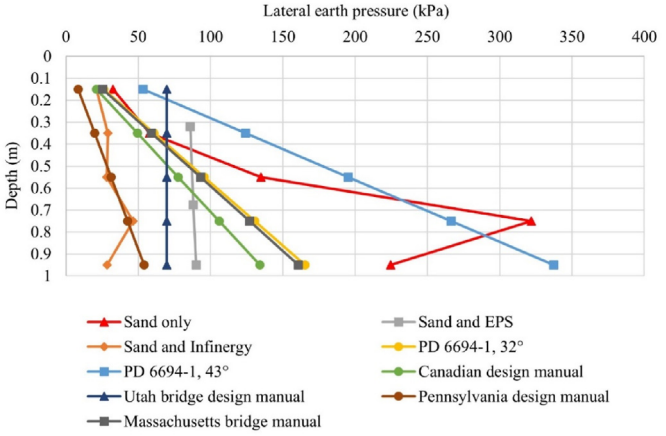

Fig. 20. Comparison of maximum earth pressure envelope along the height of the wall (up to 50 cycles) with different practices.

Table 4
Comparison of transferred displacement at Infinergy®-soil interface.

Passive displacement (mm)	Interface displacement (mm) at following thickness of Infinergy®				Percentage of transferred displacement (%) (experiment = 300 mm)	Percentage of transferred displacement at following thickness of Infinergy® (%)		
	Experiment = 300 mm	FEM				FEM		
		300 mm	450 mm	600 mm		300 mm	450 mm	600 mm
2.5		0.63	0.6	0.57		25	24	23
5	1	1.05	0.79	0.59	20	21	16	12
7.5		1.18	0.82	0.59		16	11	8
10	1.5	1.4	0.85	0.6	15	14	9	6
12.5		1.74	0.88	0.61		14	7	5
15	2.5	2.29	0.95	0.63	17	15	6	4
17.5		2.94	1.01	0.68		17	6	4
20	5	4.92	1.2	0.71	25	25	6	4

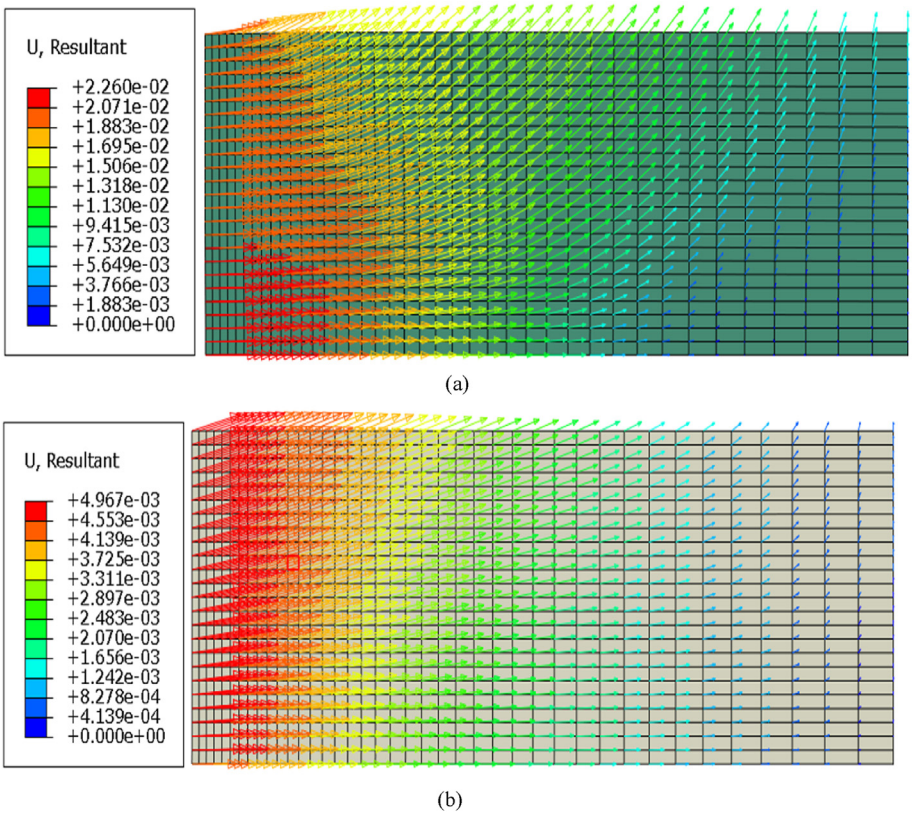

Fig. 21. Resultant soil movement after 20 mm of monotonic passive displacement: (a) Sand only, and (b) Sand and Infinergy® (Note: all dimensions are in m).

further examine the displacement of the abutment transferred to the soil under cyclic translational movements in presence of Infinergy® inclusion, a monotonic passive translational displacement experiment was conducted on the semi-scale model tank.

A two-dimensional (2D) plane strain FEM using the Abaqus FE program was also developed, to simulate a 0.96 m high abutment wall retaining a 300 mm thick Infinergy® inclusion layer and soil backfill. A Four-node bilinear plane strain quadrilateral element type was selected for the FEM and Abaqus/explicit analysis was performed using an interval of 2.5 mm monotonic passive translational movements (see Table 4) up to 20 mm. Numerous studies have been carried out using the Hyperelastic constitutive models for rubber and foam-like materials (Swanson, 1985; Bergström and Boyce, 1998; Steinmann et al., 2012). The stress-strain response for

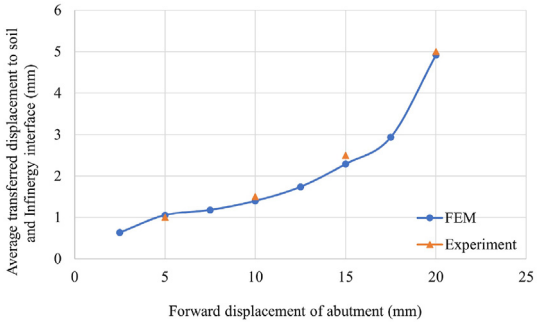

Fig. 22. Transferred displacement to Infinergy®-soil interface (mm).

Hyperelastic material is nonlinear in nature, and increases monotonically until failure, as shown in Figs. 2 and 3 for Infinergy®. This material model enables the internal energy stored in the material to be fully recovered after unloading if it is within the elastic limit. The Hyperelastic material model is available in Abaqus FE program, and it allows using the material test data to define the deviatoric and volumetric responses of the material under deformation. Therefore, Hyperelastic material model was used for the Infinergy®, based on the material tests conducted on both materials, and Mohr-Coulomb model was adopted for the Black sand behind the wall. The interactions between the interfaces (Infinergy® and sand, Infinergy® and wall) were modelled using the contact algorithm in Abaqus/Standard, where a penalty friction formulation with finite sliding for the tangential behaviour and hard contact for the normal behaviour has been adopted. Friction angles 15° and 20° were used to model the interfaces of Black sand-Infinergy® and wall-Infinergy®, respectively. The gravity load and predefined initial stresses were defined at the initial step and propagated into the latter gravity and loading steps. Passive displacement as per the test requirement was provided using the boundary conditions. The FEM results of the soil movements for the soil without and with Infinergy® are shown in Fig. 21.

Experimental data show that the Infinergy® inclusion has clearly mitigated the abutment displacement transferred to the backfill soil. The average transferred displacement at the interface of backfill soil/Infinergy® observed from the experiment is compared with FEM results as shown in Table 4. Both experimental and FEM results show that the transferred movement was about 14%–25% of the abutment wall displacement for 300 mm thick Infinergy® (Fig. 22 and Table 4). Therefore, the experimental results validate the predicted transferred displacements of the FEM model.

FEM analysis has then extended to 450 mm and 600 mm thick Infinergy® to study how the transferred displacement would be further mitigated by increasing the thickness of Infinergy®. Based on the FEM results, increasing the thickness of Infinergy® by 1.5 times (to 450 mm), the transferred displacement is now about 6%–24% of the abutment wall displacement, compared to 15%–25% for the Infinergy® of 300 mm thickness (Table 4). Furthermore, by increasing the thickness of Infinergy® by twice (to 600 mm), the transferred displacement is about 4%–23% of the abutment wall displacement. These results would suggest that beyond a certain optimal thickness, the reduction of transferred displacement with increased Infinergy® thickness would be marginal.

4.2.4. Cost comparison

The total cost associated with the construction of an integral bridge is determined by many factors, including the construction and material cost, maintenance cost, social cost, the economics of scale, and environmental cost. Therefore, a cost analysis and direct cost comparison of backfill design options (e.g. EPS geofoam versus Infinergy® versus mechanically stablised wall (MSW)) are fraught with difficulties. However, the use of compressible inclusions can reduce the maintenance cost and any other costs arising from road closures to repair the bridge approach due to settlement issues of integral bridges. In addition, both types of compressible inclusions discussed in this paper are lightweight materials compared to conventional fill materials and hence benefit from the reduction of the material handling cost involved with equipment and manpower. Another cost benefit is the savings due to the reduction of overall project duration. It is noteworthy to point out that the significant reduction in earth pressure development behind the abutment due to abutment movements can also reduce the construction cost of the superstructural and substructural elements. Since cost is another critical aspect to be studied and needs rigorous analysis, further research is required to incorporate the cost analysis with different backfill design options to help in the selection of the optimal solution.

5. Conclusions

This paper studied the interactions of integral bridge abutment and backfill due to cyclic translational movement for three different backfill conditions: (a) sand only as backfill, (b) sand and EPS geofoam inclusion, and (c) sand and Infinergy® inclusion. The backfill settlement profile and the earth pressure distribution behind the abutment wall were investigated and compared. Based on the results presented in this paper, the following conclusions can be drawn:

(1) Infinergy® as a compressible inclusion is a better alternative than the EPS geofoam, as it worked more effectively to reduce the soil settlement and heaving, as well as soil, ratcheting effects under cyclic translational movement. For a cyclic translational movement of ±10 mm and when 300 mm thick Infinergy® was used, the maximum soil settlement reduced to approximately 18.6% and soil settlement trough area to about 8.6% of those without inclusion after 120 cycles. A maximum earth pressure of 325 kPa was developed for the compacted sand-only backfill as opposed to only 47 kPa for the backfill with the Infinergy® inclusion.
(2) Medium density EPS geofoam also performed relatively well concerning the earth pressure behind the abutment wall. However, soil deformation was still significantly high, despite the thickness of the EPS block being double that of the Infinergy® layer.
(3) Based on the measured interface displacement and FEM analysis, Infinergy® has the potential to absorb a significant percentage of applied displacement while transferring the remaining to the backfill. It is surmised based on experimental results that in a field scale of 1.92 m high abutment using 600 mm thick Infinergy® inclusion, 75%–85% of 20 mm applied displacement would be absorbed with the remaining 15%–25% transferred to the backfill.
(4) FEM modelling results also suggest that beyond an optimal thickness of Infinergy® inclusion, the reduction in transferred displacement would be marginal.
(5) The use of Infinergy® as a compressible inclusion has the potential to reduce significant cost of abutment and backfill construction. In addition, Infinergy® is recyclable, has good chemical resistance, is long-term durable over a wide range of temperatures, sustainable, and non-hazardous. These attributes are favourable to the environment.
(6) The study suggests that the conventional passive pressure coefficient K_p which is derived from monotonic passive wall movement, is not an accurate predictor of the passive pressures caused by cyclic wall movements, such as in an integral bridge abutment.
(7) Most of the design practices including PD 6694-1 (2020), CAN/CSA-S6-14 (2015), and MassDOT (2020) have suggested that for cyclic translational movement, the design pressure distribution behind the integral abutment wall is a right-angle triangle with the maximum earth pressure at the bottom of the abutment. The results in this paper show that

the pressure distribution has a peak value in the lower half of the abutment, but not at the bottom.

Declaration of competing interest

The authors declare that they have no known competing financial interests or personal relationships that could have appeared to influence the work reported in this paper.

Acknowledgments

The authors gratefully acknowledge and thank BASF for providing the Infinergy® material used in this research. The continuous technical support provided by Mr. Van Doan and Advanced Materials Characterisation Facility (AMCF) at Western Sydney University (WSU) are also gratefully acknowledged. This research is supported by the Graduate student research fund of WSU. This research did not receive any specific grant from funding agencies in the public, commercial, or not-for-profit sectors.

References

Al-qarawi, A., Leo, C., Liyanapathirana, D., Ekanayake, S., 2016. A study on the effects of abutment cyclic movements on the approach of integral abutment bridges. Aust. Geomech. 51 (2), 1–3.
Al-qarawi, A., Leo, C.J., Liyanapathirana, S., 2020. Effects of wall movements on performance of integral abutment bridges. Int. J. GeoMech. 20 (2), 1–14.
Al-qarawi, A., 2021. A Study on the Fundamental Behaviour of Soil-Structure Interaction and Mitigating Effects of EPS Geofoam Inclusions in Integral Abutment Bridges. PhD Thesis. Western Sydney University, Sydney, NSW, Australia.
Al-qarawi, A., Leo, C.J., Liyanapathirana, S., Sigdel, L., Lu, M., Hu, P., 2021. A spreadsheet-based technique to calculate the passive soil pressure based on the log-spiral method. Comput. Geotech. 130, 103926.
Argyroudis, S., Palaiochorinou, A., Mitoulis, S., Pitilakis, D., 2016. Use of rubberised backfills for improving the seismic response of integral abutment bridges. Bull. Earthq. Eng. 14 (12), 3573–3590.
AS 5100-2017, 2017. Australian Bridge Design Code. Standards Australia, Sydney, NSW, Australia, 2017.
ASTM D4253-16e1, 2016. Standard Test Methods for Maximum Index Density and Unit Weight of Soils Using a Vibratory Table. ASTM International, West Conshohocken, PA, USA.
ASTM D4254-00, 2000. Standard Test Methods for Minimum Index Density and Calculation of Relative Density (RD): Designation. ASTM International, West Conshohocken, PA, USA.
Aziman, M., Saifulnaz, M.R., Hejazi, F., Azarkerdar, A., 2019. Formation of bridge end bumps due to settlement at bridge approaches. IOP Conf. Ser. Earth Environ. Sci. 357 (1), 1–9.
Bergström, J.S., Boyce, M.C., 1998. Constitutive modeling of the large strain time-dependent behavior of elastomers. J. Mech. Phys. Solid. 46 (5), 931–954.
CAN/CSA-S6-14, 2015. Canadian highway bridge design code. Canadian standards association, ottowa. Micromed, tromino user's manual. Micro 139.
Carder, D., Card, G., 1997. Innovative Structural Backfills to Integral Bridge Abutments. Transport Research Laboratory, Crawthorne, UK.
Colorado Bridge Design Manual, 2023. Colorado Department of Transportation, Colorado, USA. https://www.codot.gov/programs/bridge/bridgemanuals/design_manual.
Cosgrove, E.F., Lehane, B.M., 2003. Cyclic loading of loose backfill placed adjacent to integral bridge abutments. Int. J. Phys. Model. 3 (3), 09-16.
Cui, L., Mitoulis, S., 2015. DEM analysis of green rubberised backfills towards future smart Integral Abutment Bridges (IABs). Geomechanics from Micro to Macro. I. II 583–588.
Duda, A., Siwowski, T., 2020. Pressure evaluation of bridge abutment backfill made of waste tyre bales and shreds: experimental and numerical study. Transp. Geotech. 24, 100366.
England, G.L., Tsang, N.C., Bush, D.I., 2000. Integral Bridges: a Fundamental Approach to the Time–Temperature Loading Problem. Highways Agency. Thomas Telford Publishing, London, UK, pp. 1–176.
Gade, V.K., Dasaka, S., 2022. Short-and long-term behavior of EPS geofoam in reduction of lateral earth pressure on rigid retaining wall subjected to surcharge loading. Geotext. Geomembranes 50 (5), 868–880.
Ge, C., Ren, Q., Wang, S., Zheng, W., Zhai, W., Park, C.B., 2017. Steam-chest molding of expanded thermoplastic polyurethane bead foams and their mechanical properties. Chem. Eng. Sci. 174, 337–346.
Goh, C.T., 2001. The Behaviour of Backfill to Shallow Abutments of Integral Bridges. PhD Thesis. University of Birmingham, UK.
Hazarika, H., Kohama, E., Sugano, T., 2008. Underwater shake table tests on waterfront structures protected with tire chips cushion. J Geotech Geoenviron 134 (12), 1706–1719.
Hoppe, E.J., 2005. Field Study of Integral Backwall with Elastic Inclusion. Tech Report. FHWA/VTRC 05-R28. Transportation Research Council, Virginia. https://rosap.ntl.bts.gov/view/dot/19683.
Horvath, J.S., 1997. The compressible inclusion function of EPS geofoam. Geotext. Geomembranes 15 (1–3), 77–120.
Horvath, J.S., 2000. Integral-abutment Bridges: Problems and Innovative Solutions Using EPS Geofoam and Other Geosynthetics. CE/GE-00-2. Manhattan College, Bronx, New York, USA.
Jiang, J., Zhou, M., Li, Y., Chen, B., Tian, F., Zhai, W., 2022. Cell structure and hardness evolutions of TPU foamed sheets with high hardness via a temperature rising foaming process. J. Supercrit. Fluids 188, 105654.
Lee, H.J., Roh, H.S., 2007. The use of recycled tire chips to minimise dynamic earth pressure during compaction of backfill. Construct. Build. Mater. 21 (5), 1016–1026.
Leo, C.J., Ameratunge, J., Taylor, B., Patten, M., 2007. EPS geofoam: an engineering material for geotechnical applications. In: Common Ground: Proceedings of the 10Th Australia New Zealand Conference on Geomechanics: Australian Geomechanics Society and the New Zealand Geotechnical Society Inc. (Hilton Hotel, Brisbane, Queensland, Australia).
Liberzon, A., Käufer, T., Bauer, A., Vennemann, P., Zimmer, E., 2021. OpenPIV/openpiv-python: OpenPIV-Python v0.23.6 (0.23.6). Zenodo. https://doi.org/10.5281/zenodo.5009150.
MassDOT, 2020. LRFD Bridge Design Manual—Part I, n.d. Massachusetts Department of Transportation, Boston, MA, USA. https://www.mass.gov/info-details/part-i-design-guidelines.
Munoz, H., Tatsuoka, F., Hirakawa, D., et al., 2012. Dynamic stability of geosynthetic-reinforced soil integral bridge. Geosynth. Int. 19 (1), 11–38.
Ng, C.W., Springman, S.M., Norrish, A.R., 1998. Centrifuge modeling of spread-base integral bridge abutments. J. Geotech. Geoenviron. 124 (5), 376–388.
PD 6694-1, 2020. Recommendations for the Design of Structures Subject to Traffic Loading to BS EN 1997-1:2004+A1:2013. BSI (British Standard International), London, UK.
Pennsylvania Bridge Design Manual, Part 4, 2019. Pennsylvania department of transportation. Harrisburg, PA, USA. https://www.penndot.pa.gov/ProjectAndPrograms/Bridges/Pages/Plans,-Standards-and-Specifications.aspx.
Prissok, F., Braun, F., Basf, S.E., 2010. Foams based on thermoplastic polyurethanes. U.S. Patent Application 12/161, 354.
Sigdel, L.D., Al-qarawi, A., Leo, C.J., Liyanapathirana, S., Hu, P., Don, V., 2021a. Response of approach to integral abutment bridge under cyclic thermal movement. In: Proceedings of the 6th GeoChina International Conference on Civil and Transportation Infrastructures: from Engineering to Smart and Green Life Cycle Solutions-2020. Springer International Publishing, Nanchang, China, pp. 1–17.
Sigdel, L.D., Al-qarawi, A., Leo, C.J., Liyanapathirana, S., Hu, P., 2021b. Geotechnical design practices and soil–structure interaction effects of an integral bridge system: a review. Appl. Sci. 11 (15), 7131.
Springman, S., Norrish, A., Ng, C., 1996. Cyclic loading of sand behind integral bridge abutments. TRL REPORT 146, 1–69.
Steinmann, P., Hossain, M., Possart, G., 2012. Hyperelastic models for rubber-like materials: consistent tangent operators and suitability for Treloar's data. Arch. Appl. Mech. 82 (9), 1183–1217.
Swanson, S.R., 1985. A constitutive model for high elongation elastic materials. J. Eng. Mater. Trans. ASME 107, 110–115.
Tapper, L., Lehane, B., 2005. Lateral Stress Development on Integral Bridge Abutments. CRC Press/Balkema, pp. 1069–1075.
Tatsuoka, F., Hirakawa, D., Nojiri, M., et al., 2009. A new type of integral bridge comprising geosynthetic-reinforced soil walls. Geosynth. Int. 16 (4), 301–326.
Utah Bridge Design Manual, 2017. Utah Department of Transportation, Salt Lake City, UT, USA. https://www.udot.utah.gov/connect/?s=Utah+Bridge+Design+Manual.
Virginia Bridge Design Manual, 2020. Virginia Department of Transportation, Virginia, USA. https://www.virginiadot.org/business/bridge-manuals.asp.

Mr. Lila Dhar Sigdel is currently pursuing PhD at Western Sydney University (WSU), Sydney, Australia, specialised in geotechnical engineering. He obtained his MSc degree from WSU and BSc degree of Civil Engineering from Tribhuvan University, Nepal. Lila Dhar Sigdel is a geotechnical engineer with a demonstrated history of working on complex geotechnical and civil engineering projects and in the higher education industry in Australia.